Proceedings of HT2009
2009 ASME Summer Heat Transfer Conference
July 19-23, 2009, San Francisco, California, USA

HT2009-88211

REDUCED BASIS METHODS AND A POSTERIORI ERROR ESTIMATORS FOR HEAT TRANSFER PROBLEMS[§]

G. Rozza[*]
Modelling and Scientific Computing, CMCS
Ecole Polytechnique Fédérale de Lausanne, EPFL
Station 8-MA, Lausanne
CH-1015, Switzerland
Email: gianluigi.rozza@epfl.ch

C. N. Nguyen
Department of Aeronautics and Astronautics,
Massachusetts Institute of Technology, MIT,
Room 37-435, 77 Massachusetts Avenue,
Cambridge, MA 02139, US
Email: cuongng@mit.edu

A.T. Patera
Department of Mechanical Engineering,
Massachusetts Institute of Technology, MIT,
Room 3-266, 77 Massachusetts Avenue,
Cambridge, MA 02139, US
Email: patera@mit.edu

S. Deparis
Modelling and Scientific Computing, CMCS
Ecole Polytechnique Fédérale de Lausanne, EPFL
Station 8-MA, Lausanne
CH-1015, Switzerland
Email: simone.deparis@epfl.ch

ABSTRACT

This paper focuses on the parametric study of steady and unsteady forced and natural convection problems by the certified reduced basis method. These problems are characterized by an input-output relationship in which given an input parameter vector — material properties, boundary conditions and sources, and geometry — we would like to compute certain outputs of engineering interest — heat fluxes and average temperatures. The certified reduced basis method provides both (i) a very inexpensive yet accurate output prediction, and (ii) a rigorous bound for the error in the reduced basis prediction relative to an underlying expensive high-fidelity finite element discretization. The feasibility and efficiency of the method is demonstrated for three natural convection model problems: a scalar steady forced convection problem in a rectangular channel is characterized by two parameters — Péclet number and the aspect ratio of the channel — and an output – - the average temperature over the domain; a steady natural convection problem in a laterally heated cavity is characterized by three parameters — Grashof and Prandtl numbers, and the aspect ratio of the cavity — and an output — the inverse of the Nusselt number; and an unsteady natural convection problem in a laterally heated cavity is characterized by two parameters — Grashof and Prandtl numbers— and a time-dependent output — the average of the horizontal velocity over a specified area of the cavity.

Keywords Reduced basis method, error estimators, steady and unsteady heat transfer, natural and forced convection, parametrized systems, Graetz flow, Péclet number, Grashof number, and Prandtl number.

[*]Corresponding author (G. Rozza is research affiliate at MIT). [§]We thank Dr. D.B. Phuong Huynh (Singapore-MIT Alliance) and Dr. Paul Fisher (Argonne National Lab.) for their collaboration and we acknowledge Dr. Karen Veroy-Grepl and Dr. Martin Grepl (formerly at MIT) for their previous contributions on natural convection. We thank the MIT Mechanical Engineering Pappalardo Book Fund for support of the educational components of this project. The development of the computational methodology is supported by AFOSR Grant No FA9550-05-1-0114 and FA-9550-07-1-0425.

1 INTRODUCTION

Several processes in convective heat and mass transfer can be modeled by parametrized partial differential equations (PDEs). Engineering analysis of these processes requires prediction of certain outputs of interest for any given instance of the parameter input vector. The *input-parameter* vector may characterize either the geometric configuration, some physical properties, or boundary conditions and source terms. The *outputs of interest* may be the maximum or average system temperature, or a heat flux, or a channel flowrate or pressure drop. These outputs may be best articulated as functionals of the *field variables* of the underlying PDEs, which typically represent velocity, pressure, and temperature.

There are many examples of reduced order models not only for linear and nonlinear heat transfer (conduction) problems [22] but also for fluid dynamics and Boussinesq natural convection flows [5, 11, 15, 16, 24]. The reduced order model can often capture the desired system input–output behavior accurately; furthermore, at least for systems with only quadratic nonlinearities — such as the Boussinesq equations — the reduced order model can be significantly less costly than high-fidelity models obtained by classical discretization techniques such as the finite element method. However, *parametric certified* reduced order models for nonlinear PDEs are generally not available due to both (*i*) lack of uniform convergence in the parameter domain — hence typically only time or at most one parameter is considered, and (*ii*) lack of rigorous error bounds — of the many earlier examples of reduced order models for the incompressible Navier-Stokes and Boussinesq equations [5, 11, 15, 24], none is endowed with *rigorous* error estimators.

In this paper we discuss a parametric certified reduced basis approach — built upon an underlying "truth" finite element discretization which we wish to accelerate — that provides both reliable results and rapid response in the real-time and many-query contexts. Reliability is ensured by rigorous a posteriori bounds for the error in the reduced basis approximation relative to the truth finite element discretization: in particular, we provide error bounds for the outputs of interest. Rapid response is ensured by an Offline–Online computational strategy that minimizes marginal cost: in an expensive Offline stage we prepare a very small reduced basis "database"; in the Online stage, for each new parameter value of interest, we rapidly evaluate both the output of interest and the associated a posteriori error bound in complexity independent of the dimensionality of the truth finite element approximation space.

The essential ingredients of our parametric certified reduced basis approach are Galerkin projection onto a low-dimensional space associated with a smooth parametric manifold — to provide dimension reduction [1, 21, 23, 25, 30]; an efficient Greedy sampling method for identification of optimal and numerically stable approximations [18, 30] — to yield rapid convergence; accurate (Online) calculation of the stability factor by the Successive Constraint Method [13, 19] — to quantify the growth of residuals; rigorous *a posteriori* error bounds for the errors in the reduced basis approximation and associated outputs — to provide *certainty* in our predictions; and an Offline-Online computational decomposition strategy for our reduced basis approximation and associated error bound [29] — to minimize marginal cost for high performance in the real-time (e.g., parameter-estimation, control) and many-query (e.g., design optimization, stability map) contexts.

In this paper we describe our work on certified reduced basis methods for steady and unsteady conduction [10, 25, 29, 30], steady and unsteady forced convection [30], and steady and unsteady natural convection [6, 7, 17, 18, 34]. As we already report in [29] on steady and unsteady conduction, we choose here a complementary emphasis: forced and natural convection. In Section 2 we review the certified reduced basis approach. In Section 3 we present results for a (prescribed velocity) steady forced convection problem — a Graetz problem, and for steady and unsteady natural convection problems — enclosure flows.

2 A BRIEF OVERVIEW ON CERTIFIED REDUCED BASIS METHOD

Given space restrictions we summarize the reduced basis approach only for (steady and unsteady) natural convection. We refer the reader to the previous work [6, 7, 17, 18, 20, 34] and references therein for further details.

The reduced basis (RB) approximation is built upon, and the error in the RB approximation is measured relative to, a high–fidelity (expensive) "truth" finite element approximation. We shall denote the truth finite element approximation space of dimension $\mathcal{N}$ as $X^{\mathcal{N}} \subset X$; here X is the function space over the domain Ω associated with weak formulation of the continuous problem — for example, $H_0^1(\Omega)$ for a simple scalar conduction/convection problem with homogeneous temperature boundary conditions. Note for the particular case of Navier–Stokes or Boussinesq natural convection we may consider either "mixed" spaces or divergence–free spaces

The point of departure for the RB approximation is the set of hierarchical RB approximation subspaces $X_N \equiv \text{span}\{\xi_n, 1 \leq n \leq N\}, \quad 1 \leq N \leq N_{\max}$, where $\xi_n \in X^{\mathcal{N}}, 1 \leq n \leq N_{\max}$, is a set of mutually $(\cdot,\cdot)_X$-orthogonal basis functions. In actual practice, the spaces $X_N \subset X^{\mathcal{N}}$ will be generated by a Greedy sampling procedure which combines spatial snapshots in parameter [30] (or for unsteady problems POD-Greedy sampling procedure which combines spatial snapshots in time and parameter [18]) in an optimal fashion; for our present purposes, however, X_N can in fact represent any sequence of (low-dimensional) hierarchical approximation spaces [30]. It immediately follows that $X_N \subset X^{\mathcal{N}}$, and we may hence pursue a Galerkin projection with respect to the space X_N.

2.1 Steady Natural Convection

In this section we summarize our approach to a general class of quadratically nonlinear problems that are "inf–sup" stable in an appropriate sense. Our steady natural convection problem — presented in strong form in the Section 3.2.1 — is a particular instance of this framework, though there are certain aspects of the Navier–Stokes system (in particular related to stable treatment of the pressure) that require special treatment [26, 31].

For simplicity in our description we consider only homogeneous Dirichlet (wall) boundary conditions: thus the velocity space Y is the space of all functions $\boldsymbol{u} = (u_1, u_2) \in (H^1(\Omega)_0)^2$ that vanish on selected segments of the boundary; the temperature space W is the space of all functions in $H^1(\Omega)$ that vanish on the left and right walls; we also introduce the pressure space $M \equiv L^2_0(\Omega)$ of all functions q in $L^2(\Omega)$ functions of zero mean over Ω. We then define $X \equiv Y \times W \times M$; note that for any member w of X the first two components w_1 and w_2 refer to x_1 and x_2 components of velocity, respectively, while the last two components w_3 and w_4 refers to temperature and pressure, respectively. We next associate to X the inner product $(w,v)_X = \int_\Omega \frac{\partial w_i}{\partial x_j}\frac{\partial v_i}{\partial x_j}(1 \le i \le 3, 1 \le j \le 2) + \int_\Omega w_4 v_4$ and induced norm $\|\cdot\|_X = \sqrt{(\cdot,\cdot)_X}$ for $w = (w_1, w_2, w_3, w_4) \in X$ and $v = (v_1, v_2, v_3, v_4) \in X$.

We can now state the parametrized weak formulation of the steady Boussinesq equations: for given $\boldsymbol{\mu}$ in the parameter domain $\mathcal{D}$, the velocity-temperature-pressure field $u(\boldsymbol{\mu}) \equiv (u_1(\boldsymbol{\mu}), u_2(\boldsymbol{\mu}), T(\boldsymbol{\mu}), p(\boldsymbol{\mu})) \in X$ satisfies

$$\mathcal{A}(u(\boldsymbol{\mu}), v; \boldsymbol{\mu}) = f(v; \boldsymbol{\mu}), \forall v \in X. \tag{1}$$

As usual, the form $\mathcal{A}$ includes diffusion, buoyancy, convection, and incompressibility, and the functional f represents the forcing term. Our particular interest is not in the solution field *per se*, but rather in the output s which is defined as a linear functional ℓ of the solution $s(\boldsymbol{\mu}) = \ell(u(\boldsymbol{\mu}); \boldsymbol{\mu})$. We may also readily consider quadratic outputs, however efficient treatment of more general nonlinear outputs requires additional ingredients [9].

We shall assume that $\mathcal{A}$ is affine in the parameter $\boldsymbol{\mu}$: in particular, for some finite Q_0 and Q_1 the form $\mathcal{A}\colon X \times X \to \mathbb{R}$ can be expressed as

$$\mathcal{A}(u, v; \boldsymbol{\mu}) = \sum_{q=1}^{Q_0} \Theta_0^q(\boldsymbol{\mu}) \mathcal{A}_0^q(u, v) + \frac{1}{2}\sum_{q=1}^{Q_1} \Theta_1^q(\boldsymbol{\mu}) \mathcal{A}_1^q(u, u, v), \tag{2}$$

for u, v in X and $\boldsymbol{\mu}$ in $\mathcal{D}$, where $\Theta_0^q, \Theta_1^q\colon \mathcal{D} \to \mathbb{R}$ are parameter-dependent continuously differentiable functions and $\mathcal{A}_0^q\colon X \times X \to \mathbb{R}$, $1 \le q \le Q_0$, and $\mathcal{A}_1^q\colon X \times X \times X \to \mathbb{R}$, $1 \le q \le Q_1$, are parameter-independent continuous bilinear and trilinear forms. We also assume that the functionals f and ℓ satisfy a similar affine decomposition. The affine assumption (2) is crucial to the performance of the Offline-Online computational decomposition and is satisfied by our numerical examples in the next section.

We next denote by $X^{\mathcal{N}}$ the standard conforming $\mathbb{P}_2 - \mathbb{P}_2 - \mathbb{P}_1$ (quadratic/quadratic/linear) velocity-temperature-pressure Taylor-Hood finite element approximation subspace of X over a uniform "triangulation" of Ω; note that $X^{\mathcal{N}}$ is of dimension $\mathcal{N}$. We can now define the FE approximation for (1): for given $\boldsymbol{\mu}$ in the parameter domain $\mathcal{D}$ we look for $u^{\mathcal{N}}(\boldsymbol{\mu}) \in X^{\mathcal{N}}$ such that

$$\mathcal{A}(u^{\mathcal{N}}(\boldsymbol{\mu}), v; \boldsymbol{\mu}) = f(v; \boldsymbol{\mu}), \quad \forall v \in X^{\mathcal{N}}. \tag{3}$$

We then evaluate the output of interest $s^{\mathcal{N}}(\boldsymbol{\mu}) = \ell(u^{\mathcal{N}}(\boldsymbol{\mu}); \boldsymbol{\mu})$.

We denote by $X_N \subset X^{\mathcal{N}}$ the RB space of dimension N. Our RB approximation with respect to (3) can be stated as: for given $\boldsymbol{\mu}$ in $\mathcal{D}$, we find $u_N(\boldsymbol{\mu}) \in X_N$ such that

$$\mathcal{A}(u_N(\boldsymbol{\mu}), v; \boldsymbol{\mu}) = f(v; \boldsymbol{\mu}), \quad \forall v \in X_N. \tag{4}$$

We then apply Newton iteration to find $u_N(\boldsymbol{\mu})$: if we denote the current Newton iterate as $\overline{u}_N(\boldsymbol{\mu})$ then the Newton increment $\delta\overline{u}_N(\boldsymbol{\mu})$ satisfies

$$D\mathcal{A}(\overline{u}_N(\boldsymbol{\mu}); \boldsymbol{\mu})(\delta\overline{u}_N(\boldsymbol{\mu}), v) = f(v; \boldsymbol{\mu}) - \mathcal{A}(\overline{u}_N(\boldsymbol{\mu}), v; \boldsymbol{\mu})\ \forall v \in X_N; \tag{5}$$

here $D\mathcal{A}(w; \boldsymbol{\mu})(u, v)$ is the Frechet derivative of $\mathcal{A}(u, v; \boldsymbol{\mu})$ at the current point w and is given by

$$D\mathcal{A}(w; \boldsymbol{\mu})(u, v) = \sum_{q=1}^{Q_0} \Theta_0^q(\boldsymbol{\mu}) \mathcal{A}_0^q(u, v) + \sum_{q=1}^{Q_1} \Theta_1^q(\boldsymbol{\mu}) \mathcal{A}_1^q(u, w, v). \tag{6}$$

The next iterate is then given by $\overline{u}_N(\boldsymbol{\mu}) + \delta\overline{u}_N(\boldsymbol{\mu})$; we continue until convergence. The linearized problem (5) can be treated efficiently by an Offline-Online decomposition as described below.

The Offline-Online computational decomposition relies on the affine assumption of our form $\mathcal{A}$. We first express $\overline{u}_N(\boldsymbol{\mu}) = \sum_{n=1}^N \overline{c}_{Nn}(\boldsymbol{\mu})\xi_n$, $\delta\overline{u}_N(\boldsymbol{\mu}) = \sum_{j=1}^N \delta\overline{c}_{Nj}(\boldsymbol{\mu})\xi_j$, and choose $v = \xi_i$ in (5) to obtain

$$D\mathcal{A}(\overline{u}_N(\boldsymbol{\mu}); \boldsymbol{\mu})(\delta\overline{u}_N(\boldsymbol{\mu}), \xi_i) = \sum_{j=1}^N \left(\sum_{q=1}^{Q_0} \Theta_0^q(\boldsymbol{\mu}) \mathcal{A}_0^q(\xi_j, \xi_i) + \sum_{n=1}^N \sum_{q=1}^{Q_1} \Theta_1^q(\boldsymbol{\mu}) \overline{c}_{Nn}(\boldsymbol{\mu}) \mathcal{A}_1^q(\xi_j, \xi_n, \xi_i) \right) \delta\overline{c}_{Nj}(\boldsymbol{\mu}). \tag{7}$$

The Offline-Online decomposition is now clear: in the Offline stage, we can form and store $\mathcal{A}_0^q(\xi_j,\xi_i)$ and $\mathcal{A}_1^{q'}(\xi_j,\xi_n,\xi_i), 1 \le i,j,n \le N, 1 \le q \le Q_0, 1 \le q' \le Q_1$, with $\mathcal{N}$-dependent cost, since these quantities are $\boldsymbol{\mu}$-independent; in the Online stage, we perform the sum in the parenthesis of (7) in only $Q_0N^2 + Q_1N^3$ operations. The Offline-Online decomposition for the functionals f and ℓ can be implemented in the same manner.

To provide *a posteriori* error bound for the error in the solution, we apply the Brezzi-Rappaz-Raviart theory [4]. For simplicity of exposition we present the result in the X-norm, though in actual practice we incorporate a more efficient "natural norm" [6, 33]. It can be shown that the X-norm of the RB error, $||u(\boldsymbol{\mu}) - u_N(\boldsymbol{\mu})||_X$, can be bounded by

$$||u(\boldsymbol{\mu}) - u_N(\boldsymbol{\mu})||_X \le \Delta_N(\boldsymbol{\mu}) \equiv \frac{\beta^{\rm LB}(\boldsymbol{\mu})}{\rho}\left(1 - \sqrt{1-\tau_N(\boldsymbol{\mu})}\right), \quad (8)$$

where $\tau_N(\boldsymbol{\mu}) = \frac{2\rho\varepsilon_N(\boldsymbol{\mu})}{(\beta^{\rm LB}(\boldsymbol{\mu}))^2}$ and $\beta^{\rm LB}(\boldsymbol{\mu})$ is the lower bound of the inf-sup stability constant $\beta(\boldsymbol{\mu}) = \inf_{w\in X}\sup_{v\in X}\frac{d\mathcal{A}(u_N(\boldsymbol{\mu});\boldsymbol{\mu})(w,v)}{||w||_X||v||_X}$; we assume that $\beta(\boldsymbol{\mu}) > 0$ for all $\boldsymbol{\mu}$ in $\mathcal{D}$, that is, we are on an isolated solution branch without bifurcations. Note here that $\varepsilon_N(\boldsymbol{\mu}) = \sup_{v\in X^{\mathcal{N}}} r(v;\boldsymbol{\mu})/\|v\|_X$ is the dual norm of the residual $r(v;\boldsymbol{\mu}) = f(v) - \mathcal{A}(u_N(\boldsymbol{\mu}),v;\boldsymbol{\mu})$, and ρ is a constant related to the $L^4(\Omega)$-$H^1(\Omega)$ Sobolev embedding [6, 7]. The lower bound $\beta^{\rm LB}(t;\boldsymbol{\mu})$ [13, 19, 30], and the dual norm of the residual [17, 18] are also amenable to an Offline–Online computational decomposition.

It should be noted that $\Delta_N(\boldsymbol{\mu})$ is not well defined for $\beta^{\rm LB}(\boldsymbol{\mu}) < 0$ and $\tau(\boldsymbol{\mu}) > 1$. Fortunately, these conditions can be verified Online: if $\beta^{\rm LB}(\boldsymbol{\mu}) > 0$ and $\tau(\boldsymbol{\mu}) \le 1$ then our RB solution $u_N(\boldsymbol{\mu})$ is unique and satisfies (8); if $\tau(\boldsymbol{\mu}) > 1$ (i.e., we can not guarantee that $u_N(\boldsymbol{\mu})$ is close to $u^{\mathcal{N}}(\boldsymbol{\mu})$) then we enrich our RB space X_N (by increasing N) to reduce $\varepsilon_N(\boldsymbol{\mu})$ and thus render $\tau(\boldsymbol{\mu}) \le 1$.

Finally, the bound for the error in the output, $|s^{\mathcal{N}}(\boldsymbol{\mu}) - s_N(\boldsymbol{\mu})|$, is defined as $\Delta_N^s(\boldsymbol{\mu}) = \sup_{v\in X^{\mathcal{N}}}(\ell(v;\boldsymbol{\mu})/\|v\|_X)\Delta_N(\boldsymbol{\mu})$.

2.2 Unsteady Natural Convection

We assume the same spaces as the steady case. However, unlike the steady case, we shall work with incompressible velocity fields. Henceforth, our solution space X is re-defined as $X \equiv Z \times W$, where Z is the space of all *divergence-free* functions in Y; note that for any member w of X the first two components w_1 and w_2 refer to x_1 and x_2 components of velocity, respectively, while the third component w_3 refers to temperature. We next associate to X the inner product $(w,v)_X = \int_\Omega \frac{\partial w_i}{\partial x_j}\frac{\partial v_i}{\partial x_j}$ and induced norm $\|\cdot\|_X = \sqrt{(\cdot,\cdot)_X}$ for $w = (w_1,w_2,w_3) \in X$ and $v = (v_1,v_2,v_3) \in X$. We also define, for any members $w \in X$, $v \in X$, the $(L^2(\Omega))^3$ inner product $(w,v) = \int_\Omega w_i v_i$ and induced norm $\|\cdot\| = \sqrt{(\cdot,\cdot)}$. The repeated index indicates summation over the range of the index, that is, $i = 1,2,3$ and $j = 1,2$ in the above expressions.

We can now state the parametrized weak formulation of the unsteady Boussinesq equations: for given $\boldsymbol{\mu}$ in the parameter domain $\mathcal{D}$ and all times $t \in (0,t_f]$, the velocity-temperature field $u(t;\boldsymbol{\mu}) \equiv (u_1(t;\boldsymbol{\mu}),u_2(t;\boldsymbol{\mu}),T(t;\boldsymbol{\mu})) \in X$ satisfies

$$(u_t(t;\boldsymbol{\mu}),v) + a(u(t;\boldsymbol{\mu}),v;\boldsymbol{\mu}) + b(u(t;\boldsymbol{\mu}),v;\boldsymbol{\mu}) + c(u(t;\boldsymbol{\mu}),u(t;\boldsymbol{\mu}),v;\boldsymbol{\mu}) = f(v;\boldsymbol{\mu}), \quad \forall\, v \in X\ , \quad (9)$$

subject to initial condition $u(t=0;\boldsymbol{\mu}) = 0$. Note that the pressure is eliminated thanks to our divergence-free velocity (test) space. We subsequently evaluate our output of interest as $s(t;\boldsymbol{\mu}) = \ell(u(t;\boldsymbol{\mu});\boldsymbol{\mu})$. The forms a,b,c represent (roughly) diffusion, buoyancy, and convection (the pressure term vanishes thanks to the div-free space): the particular definition of our forms a,b,c and functionals f,ℓ depends on the particular problem; the strong formulation will be given later in the example of Section 3.3.

We next denote by $X^{\mathcal{N}} \in X$ the truth FE approximation of dimension $\mathcal{N}$. We can now define the semi-discrete FE approximation for (9): for given $\boldsymbol{\mu}$ in the parameter domain $\mathcal{D}$ and all times $t \in (0,t_f]$, we look for $u^{\mathcal{N}}(\boldsymbol{\mu}) \in X^{\mathcal{N}}$ such that

$$(u_t^{\mathcal{N}}(t;\boldsymbol{\mu}),v) + a(u^{\mathcal{N}}(t;\boldsymbol{\mu}),v;\boldsymbol{\mu}) + b(u^{\mathcal{N}}(t;\boldsymbol{\mu}),v;\boldsymbol{\mu}) + c(u^{\mathcal{N}}(t;\boldsymbol{\mu}),u^{\mathcal{N}}(t;\boldsymbol{\mu}),v;\boldsymbol{\mu}) = f(v;\boldsymbol{\mu}), \quad \forall\, v \in X^{\mathcal{N}}\ , \quad (10)$$

subject to initial condition $u^{\mathcal{N}}(t=0;\boldsymbol{\mu}) = 0$. We then evaluate the output of interest $s^{\mathcal{N}}(t;\boldsymbol{\mu}) = \ell(u^{\mathcal{N}}(t;\boldsymbol{\mu});\boldsymbol{\mu})$. (In actual practice we apply the Crank-Nicolson scheme for the temporal discretization of the system (10). For brevity in this paper we shall describe the RB methodology only for the semi–discrete formulation (10), however all of our results — including the rigorous error estimator — extend to fully discrete case that we actually consider in practice [17].)

We may pursue Galerkin projection with respect to (10): for given $\boldsymbol{\mu}$ in the parameter domain $\mathcal{D}$ and all times $t \in (0,t_f]$, we look for $u_N(\boldsymbol{\mu}) \in X_N$ such that

$$(u_{Nt}(t;\boldsymbol{\mu}),v) + a(u_N(t;\boldsymbol{\mu}),v;\boldsymbol{\mu}) + b(u_N(t;\boldsymbol{\mu}),v;\boldsymbol{\mu}) + c(u_N(t;\boldsymbol{\mu}),u_N(t;\boldsymbol{\mu}),v;\boldsymbol{\mu}) = f(v;\boldsymbol{\mu}), \quad \forall\, v \in X_N\ , \quad (11)$$

subject to initial condition $u_N(t=0;\boldsymbol{\mu}) = 0$. We then evaluate the RB output as $s_N(t;\boldsymbol{\mu}) = \ell(u_N(t;\boldsymbol{\mu});\boldsymbol{\mu})$.

It can be shown that the $L^2(\Omega)$ norm of the RB error,

$\|u^{\mathcal{N}}(t;\boldsymbol{\mu}) - u_N(t;\boldsymbol{\mu})\|$ can be bounded as

$$\|u^{\mathcal{N}}(t;\boldsymbol{\mu}) - u_N(t;\boldsymbol{\mu})\| \le \Delta_N(t;\boldsymbol{\mu}) \equiv \left(\int_0^{t_f} \varepsilon^2(t';\boldsymbol{\mu}) \exp(-\int_{t'}^{t} \rho_N^{\mathrm{LB}}(t'';\boldsymbol{\mu}) dt'') dt' \right)^{1/2} \quad (12)$$

where $\varepsilon(t;\boldsymbol{\mu}) = \sup_{v \in X^{\mathcal{N}}} r(v;t;\boldsymbol{\mu})/\|v\|_X$ is the dual norm of the residual $r(v;t;\boldsymbol{\mu}) \equiv f(v;\boldsymbol{\mu}) - (u_t^{\mathcal{N}}(t;\boldsymbol{\mu}),v) - a(u^{\mathcal{N}}(t;\boldsymbol{\mu}),v;\boldsymbol{\mu}) - b(u^{\mathcal{N}}(t;\boldsymbol{\mu}),v;\boldsymbol{\mu}) - c(u^{\mathcal{N}}(t;\boldsymbol{\mu}),u^{\mathcal{N}}(t;\boldsymbol{\mu}),v;\boldsymbol{\mu})$, and $\rho_N^{\mathrm{LB}}(t;\boldsymbol{\mu})$ is a lower bound for the stability constant

$$\rho_N(t;\boldsymbol{\mu}) \equiv \inf_{v \in X^{\mathcal{N}}} \frac{2c(u_N(t;\boldsymbol{\mu}),v,v;\boldsymbol{\mu}) + 2b(v,v;\boldsymbol{\mu}) + a(v,v;\boldsymbol{\mu})}{\|v\|^2}. \quad (13)$$

The error in the output, $|s^{\mathcal{N}}(t;\boldsymbol{\mu}) - s_N(t;\boldsymbol{\mu})|$, can then be bounded as

$$|s^{\mathcal{N}}(t;\boldsymbol{\mu}) - s_N(t;\boldsymbol{\mu})| \le \Delta_N^s(t;\boldsymbol{\mu}) \equiv \Big(\sup_{v \in X^{\mathcal{N}}} \frac{\ell(v;\boldsymbol{\mu})}{\|v\|} \Big) \Delta_N(t;\boldsymbol{\mu}). \quad (14)$$

In practice, our error bounds (12) and (14) inherit the Crank-Nicolson temporal discretization of the system (10).

The RB coefficients of $u_N(t;\boldsymbol{\mu})$, the output $s_N(t;\boldsymbol{\mu})$, the stability factor $\rho_N^{\mathrm{LB}}(t;\boldsymbol{\mu})$ [13,19,30], and the dual norm of the residual [17,18] are all amenable to an Offline–Online computational decomposition. In particular, the unsteady case is very similar to the steady case discussed in the the previous section: we first calculate and store a "few" quantities *once* in an Offline stage — with $O(\mathcal{N})$ complexity; we can then rapidly evaluate the output and output error bound *many times* in an Online stage — with complexity dependent on N and K (where K denotes the number of time steps in the Crank-Nicolson scheme used to discretize the time derivative) but *independent of* $\mathcal{N}$. The method is thus of interest in the real–time and many–query contexts in which the Offline stage is unimportant or amortized, respectively, and only the rapid Online stage is relevant.

Finally, we address the generation of our hierarchical RB spaces $X_N, 1 \le N \le N_{\max}$. Here we combine the POD (Proper Orthogonal Decomposition) in t — to capture the causality associated with our evolution equation — with the Greedy in $\boldsymbol{\mu}$ — to treat efficiently the higher dimensions and more extensive ranges of parameter variation [12]. In the weighted POD-Greedy approach [17–19] we first select — by inexpensive evaluation of our error bound over a large training sample — the parameter least well approximated by our current RB approximation; we then invoke the POD procedure to select optimal combinations of snapshots at this selected parameter value.

3 NUMERICAL EXAMPLES

3.1 Steady Forced Convection: Graetz Flow

In this section we introduce an example ("worked problem") dealing with steady heat (and mass) transfer: a parametrized Graetz flow [3]. Many other model problems are available at the address `http://augustine.mit.edu/workedProblems.htm` where illustrative calculations/visualization are provided by a Matlab ® webserver.

The Graetz flow is a classical problem in literature dealing with forced steady heat convection combined with heat conduction in a duct with walls at different temperature, see [2, 3, 32]. The first portion of the duct has "cold" walls, while the second portion has "hot" walls. The flow has an imposed temperature at the inlet and a known convective field (i.e. a given parabolic velocity profile). From the engineering point of view, this problem illustrates the application of conduction analysis to an important class of heat transfer problems in fluidic devices.

The domain Ω_o is given by $[0,\tilde{h}+\tilde{L}] \times [0,\tilde{h}]$ in which the region $[0,\tilde{h}] \times [0,\tilde{h}]$ is denoted the "entrance" region and $[\tilde{h},\tilde{h}+\tilde{L}] \times [0,\tilde{h}]$ is denoted the "developing" region. We further denote the boundary segment Γ_{o1} as inflow (on which we impose a temperature $\tilde{T}_{inlet}$) and the boundary segment Γ_{o4} as the outflow, the boundary segements Γ_{o2} (bottom) and Γ_{o6} (top) as the cold wall (on which we impose temperature $\tilde{T}_{inlet}$) and the boundary segments Γ_{o3} (bottom) and Γ_{o5} (top) as the hot wall (on which we impose $\tilde{T}_{hot}$). Note here $\sim$ denotes dimensional, and $_o$ refers to a parameter dependent domain. We next nondimensionalize by $\tilde{h}$ which yields the nondimensional domain Ω_o and corresponding boundary segments $\Gamma_{o.}$.

We assume that $\tilde{\kappa}$ is the dimensional thermal diffusivity for the air flowing in the duct, while $\tilde{U}$ is a reference dimensional velocity for the convective field (defined as four times the maximum velocity). We introduce the Péclet number, $Pe = \frac{\tilde{U}\tilde{h}}{\tilde{\kappa}}$. We consider here $P = 2$ parameters: μ_1 is a geometrical parameter representing the non-dimensional length of the "developing" portion of the duct $\tilde{L}/\tilde{h}$; the remaining (always non-dimensional) parameter is given by μ_2 as the Péclet number, representing the ratio between convection and conduction terms. The parameter domain is given by $\mathcal{D} = [1,10] \times [0.1,100]$.

The nondimensional temperature $T_o(\boldsymbol{\mu}) = \frac{\tilde{T}-\tilde{T}_{inlet}}{\tilde{T}_{hot}-\tilde{T}_{inlet}}$ over the nondimensional domain $\Omega_o(\boldsymbol{\mu})$ satisfies the convection–diffusion equation

$$-\frac{\partial}{\partial x_{oi}} \Bigg(\underbrace{\begin{bmatrix} {\mu_2}^{-1} & 0 \\ 0 & {\mu_2}^{-1} \end{bmatrix}}_{\kappa_{oij}} \frac{\partial T_o(\boldsymbol{\mu})}{\partial x_{oj}} \Bigg) + x_{o2}(1-x_{o2}) \frac{\partial T_o(\boldsymbol{\mu})}{\partial x_{o1}} = 0$$

with summation $(i,j = 1,2)$ over repeated indices. We note that the forced convection field is given by a parabolic (dimen-

sional) velocity profile $\tilde{x}_{o2}\left(\tilde{h}-\tilde{x}_{o2}\right)\tilde{U}$ in the x_{o1} direction. On boundaries Γ_{o1}, Γ_{o2} and Γ_{o6} we impose homogeneous Dirichlet conditions $T_o(\boldsymbol{\mu}) = 0$ (representing the imposition of the temperature in the "cold" zone of the duct and at the inlet, where the temperature of the fluid is known); on Γ_{o3} and Γ_{o5} we impose non-homogeneous Dirichlet conditions $T_o(\boldsymbol{\mu}) = 1$ (representing the imposition of the temperature in the "hot" zone of the duct); and on Γ_{o4} (outflow) we impose Neumann condition $\mathbf{n}_i \kappa_{ij} \frac{\partial T_o}{\partial x_{oj}}(\boldsymbol{\mu}) = 0$, where $\mathbf{n}_i$ denotes unit outward normal.

This problem is then mapped to a fixed reference domain Ω [29, 30] throught a piecewise affine map given by the identity in the entrance region and a dilation in the developing region; the problem is then discretized by a $\mathbb{P}_1$ finite element (FE) discretization [27] with $\mathcal{N} = 3178$ degrees of freedom. This FE approximation is typically too slow for many applications, and we hence approximate the FE prediction for the output and field variable by the reduced basis (RB) method.

We present below in Fig. 1 some representative solutions for different values of Péclet ($\mu_2 = 1$ and $\mu_2 = 100$) with $\mu_1 = 2$. Our

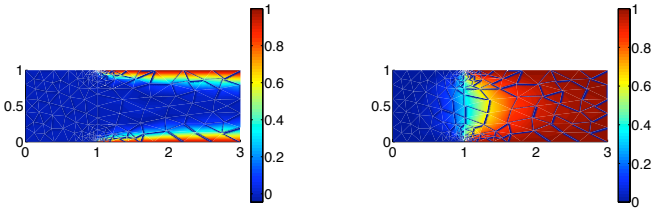

Figure 1. Representative temperature for $\mu_2 = 100$ (left) and $\mu_2 = 1$ (right) for the case $\mu_1 = 2$.

output of interest is, for simplicity, the nondimensional average temperature $T_{o\,\mathrm{av}}(\boldsymbol{\mu})$ over the domain (other outputs that could be considered include the Nusselt number on the hot wall [3]): we present in Figure 2 our results as a plot of the RB output and RB error bars — defined as the interval $[s_N(\boldsymbol{\mu}) - \Delta_N^s(\boldsymbol{\mu}), s_N(\boldsymbol{\mu}) + \Delta_N^s(\boldsymbol{\mu})]$ in which the truth FE solution *must* reside — as a function of μ_2 for $\mu_1 = 1$ and $N = 18$. To improve the accuracy of the RB prediction and effectivity of the associated error bound (in particular for this non–symmetric convection–diffusion operator) we consider a primal–dual formulation [30]; hence N refers to the number of primal modes and the number of dual modes [25, 30]. These results demonstrate the small value of N required to achieve certified high accuracy; these results also demonstrate the importance of the error bounds not only in certifying the results but also in ensuring efficiency — permitting us to *safely* choose a small value of N without sacrificing accuracy or certainty. The method also converges very quickly — increasing N to 30 reduces the certified error (maximum error bar in Figure 2) by a factor of 10^2— the error bars are no longer discernable. As regards computational times, a RB Online evalu-

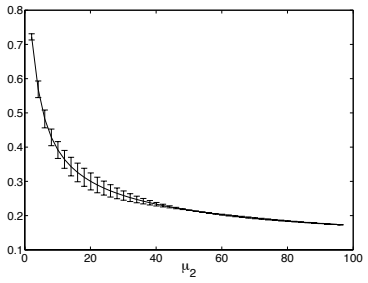

Figure 2. RB output $s_N(\boldsymbol{\mu}) = T_{o\,\mathrm{av}}(\boldsymbol{\mu})$ and RB error bars — defined as the interval $[s_N(\boldsymbol{\mu}) - \Delta_N^s(\boldsymbol{\mu}), s_N(\boldsymbol{\mu}) + \Delta_N^s(\boldsymbol{\mu})]$ — as a function of μ_2 for $\mu_1 = 1.0$, and $N = 18$.

ation requires on average 0.08s for $N = 18$ and 0.12s for $N = 30$, including both $s_N(\boldsymbol{\mu})$ and $\Delta_N^s(\boldsymbol{\mu})$; FEM solution $\boldsymbol{\mu} \rightarrow s^{\mathcal{N}}(\boldsymbol{\mu})$ requires 3.8s to be completed. Hence an average Online evaluation requires only $\sim 3\%$ of the FEM computational cost.

3.2 Natural Convection in a Laterally Heated Cavity

We consider the flow of a "Boussinesq" fluid with kinematic viscosity $\tilde{\nu}$, density $\tilde{\rho}$, thermal diffusivity $\tilde{\kappa}$, and thermal expansion coefficient $\tilde{\beta}$ in a rectangular cavity. The horizontal walls are thermally insulated. We impose no-slip velocity conditions on all four walls. This model corresponds to the benchmark case defined in [8, 28]. The Prandtl and the Grashof numbers are defined as $\mathrm{Pr} = \tilde{\nu}/\tilde{\kappa}$ and $\mathrm{Gr} = \tilde{g}\tilde{\beta}\Delta T \tilde{H}^3/\tilde{\nu}^2$, respectively, where $-\tilde{g}$ is acceleration due to gravity in the $\tilde{x}_2$-direction. Recall also that $\mathrm{Ra} = \mathrm{Gr}\,\mathrm{Pr}$ is the Rayleigh number.

We consider that the problem is already in a nondimensional form and that the cavity is a rectangular domain Ω_o of height equal to 1 and length equal to A (aspect ratio, see Figure 3). The flow is described by the momentum, continuity, and energy equations in a Cartesian coordinate system (x_{o1}, x_{o2}) for the velocity field $\boldsymbol{u}_o = (u_{o1}, u_{o2})$, the pressure p_o (perhaps eliminated via div-free spaces), and the temperature T_o.

3.2.1 Steady case We first consider a steady case where the left wall of the cavity is maintained at constant temperature $T_o = 0$ and at the right side the heat flux is constant equal to 1. The system of parameterized partial differential equations

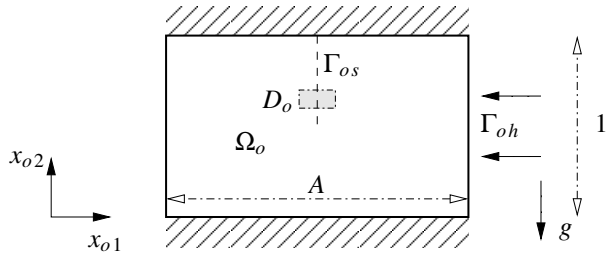

Figure 3. Enclosure geometry for the steady and unsteady natural convection problems.

in the original rectangular domain Ω_o reads

$$
\begin{aligned}
&-\frac{1}{\sqrt{\mathrm{Gr}}}\Delta \boldsymbol{u}_o + \nabla p_o + (\boldsymbol{u}_o\cdot\nabla)\boldsymbol{u}_o - T_o\begin{pmatrix}0\\1\end{pmatrix} = 0,\\
&\operatorname{div}\boldsymbol{u}_o = 0,\\
&-\frac{1}{\sqrt{\mathrm{Gr}}\,\mathrm{Pr}}\Delta T_o + (\boldsymbol{u}_o\cdot\nabla)T_o = 0.
\end{aligned}
\tag{15}
$$

We scale the pressure so that $\int_{\Omega_o} p_o = 0$. Our output of interest is the inverse of the Nusselt number [20] $s(\boldsymbol{\mu}) = \ell(T_o(\boldsymbol{\mu})) = \frac{1}{|\Gamma_{oh}|}\int_{\Gamma_{oh}} T_o(\boldsymbol{\mu})$. The parameters entering our PDE are $\boldsymbol{\mu} = (\mu_1,\mu_2,\mu_3) = (\frac{1}{\sqrt{\mathrm{Gr}}}, \frac{1}{\mathrm{Pr}\sqrt{\mathrm{Gr}}}, A)$.

We introduce our variables with respect to a reference unit square domain Ω, hence our weak form needs to incorporate a deformation in the x_1 direction. We denote with the pedix $_o$ the variables in their original domain Ω_o (which depends only on A), and without $_o$ the variables on the reference domain Ω. The form $\mathcal{A}$ defined in (2) is given by

$$
\begin{aligned}
\mathcal{A}(u,v;\boldsymbol{\mu}) = {}& \frac{\mu_1}{\mu_3}\int_\Omega \partial_1 u_j \partial_1 v_j + \mu_1\mu_3\int_\Omega \partial_2 u_j \partial_2 v_j\\
&+ \frac{\mu_2}{\mu_3}\int_\Omega \partial_1 T \partial_1 \theta + \mu_2\mu_3\int_\Omega \partial_2 T \partial_2 \theta\\
&+ \int_\Omega u_j \partial_1 u_1 v_j + \int_\Omega u_j \partial_1 u_1 v_j + \int_\Omega u_1 \partial_1 T\,\theta + \int_\Omega u_1 \partial_1 \zeta\,\theta\\
&+ \mu_3\int_\Omega u_j \partial_2 u_2 v_j + \mu_3\int_\Omega u_j \partial_2 u_2 v_j + \mu_3\int_\Omega u_2 \partial_2 T\,\theta + \mu_3\int_\Omega u_2 \partial_2 \zeta\,\theta\\
&- \int_\Omega p\partial_1 v_1 - \int_\Omega q\partial_1 u_1 - \mu_3\int_\Omega p\partial_2 v_2 - \mu_3\int_\Omega q\partial_2 u_2\\
&+ \mu_3\lambda\int_\Omega p + \mu_3\gamma\int_\Omega q - \mu_3\int_\Omega T v_2,
\end{aligned}
$$

where $\partial_i = \partial/\partial_i$, $u = (u_1,u_2,T,p,\lambda)$ and $v = (v_1,v_2,\theta,q,\gamma)$. (The extra scalar Lagrange multiplier λ enforces the zero pressure average condition.) The functional space suited for the weak formulation of our PDE is $X = H^1_0(\Omega)^2 \times H^1(\Omega) \times L^2(\Omega) \times \mathbb{R}$. The finite element "truth" approximation is modeled by a $\mathbb{P}_2 - \mathbb{P}_1 - \mathbb{P}_2$ (quadratic velocity/linear pressure/quadratic temperature) Taylor-Hood spatial discretization with a grand total of $\mathcal{N} = 38000$ degrees of freedom.

We have carried out two different test cases: in the first test we fixed A equal to 1 and let Gr and Pr vary in $[10^3, 10^5] \times [0.7, 7]$; in the second test , we fixed the Prandl number to 7 and let Gr and A vary in $[5\cdot 10^4, 7.5\cdot 10^4] \times [1.25, 1.5]$. In Figure 4 we show the temperature and the streamlines for some values of Pr and Gr. As we can see from the flows, we are considering quite different behaviors from a physical point of view.

We run the Offline process with the constraint on the parameters cited above (timing showed in Table 1). The Offline time is much larger than the time to find one FE solution, but we recall that we are interested in real-time input-ouput relationships for *a priori unknown* parameter values. The Offline time spent for the RB error bound component is much larger then for the RB output components.

We then run the Online part for many other different parameters in the same region. We have set $N = 12$, leading to a dimension of V_N equal to 50, i.e., 2 basis functions for the constant pressure and the Lagrange multipliers, N for the velocity, the temperature, and the pressure basis functions, and another N for the supremizer stabilizing the projection space [26, 31]. In Figure 5 we show the behavior of the output and its error bound on a smaller region. The triangulation has no meaning *per se*, instead each vertex represent one selected parameter for which we computed the output by the RB method. Note that although the dimension of the reduced basis is very small, the RB approximation is very accurate and is able to characterize the output with "high resolution" with respect to $\boldsymbol{\mu}$.

In Figure 6 we reported the timing and some error bound components. In the $\mathrm{Gr} - \mathrm{Pr}$ case, $\max \tau_N$ is greater than 1 for $N < 12$; this means that for some parameters in the range we do not have any proof of a nearby FE solution; when $N = 12$ $\tau(\boldsymbol{\mu})$ is smaller than 1 for all the simulations. In the $\mathrm{Gr} - A$ case the convergence of the RB approximation is very rapid. In both cases, the online time for assembling and solving the reduced basis system is proportional to N (we expected N^2, but there is a dominant linear component), while the time to compute all the error bound components is proportional to $N^{3.4}$ (due to the assembly of the dual norm of the residual, expected N^4).

3.2.2 Unsteady case The set of Boussinesq equations for the non-dimensional velocity $\boldsymbol{u}$, temperature T, and pressure

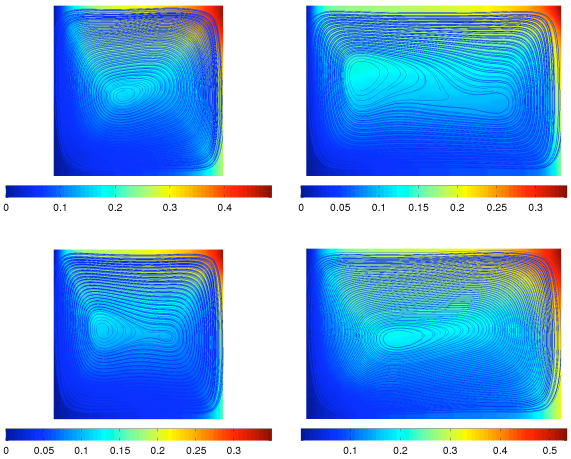

Figure 4. Temperature and (approximate) streamlines for Grashof number equal to 10^5, Prandtl number equal to 0.7 (top) and 7 (bottom), and aspect ratio equal to 1.25 (left) and 1.5 (right).

	Offline RB ($N_{\max}$)	Offline (error bound)	FE
Gr–Pr	1h44' (12)	27h15'	3'20"
Gr–A	11h24' (18)	41h48'	2'33"

Table 1. Wall times on a 16 nodes cluster; "Offline RB": computation of the reduced basis ingredients, $N_{\max}$ is the number of basis functions; "Offline (error bound)": computation of the error bound ingredients; "FE": mean time for the solution of one finite element problem.

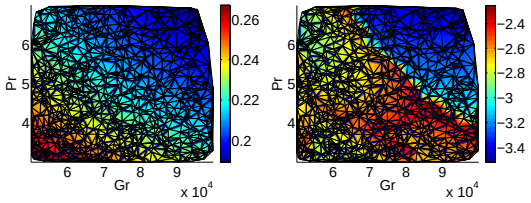

Figure 5. Output (left) and error bound (right, in logscale (base 10)) for Gr and Pr varying in the given range. A is fixed.

p for $t \in (0,t_f]$ (t_f is the final time) are given by

$$\begin{aligned}
&\frac{\partial \boldsymbol{u}}{\partial t} - \Delta \boldsymbol{u} + \sqrt{\mathrm{Gr}\,\mathrm{Pr}}\nabla p + \frac{1}{\sqrt{\mathrm{Gr}\,\mathrm{Pr}}}(\boldsymbol{u}\cdot\nabla)\boldsymbol{u} - \sqrt{\mathrm{Gr}\,\mathrm{Pr}}T\begin{pmatrix}0\\1\end{pmatrix} \\
&= \sqrt{\mathrm{Gr}\,\mathrm{Pr}}T_L\begin{pmatrix}0\\1\end{pmatrix}, \\
&\mathrm{div}\,\boldsymbol{u} = 0, \qquad (16)\\
&\frac{\partial T}{\partial t} - \frac{1}{\mathrm{Pr}}\Delta T + \frac{1}{\sqrt{\mathrm{Gr}\,\mathrm{Pr}}}(\boldsymbol{u}\cdot\nabla)T = 0.
\end{aligned}$$

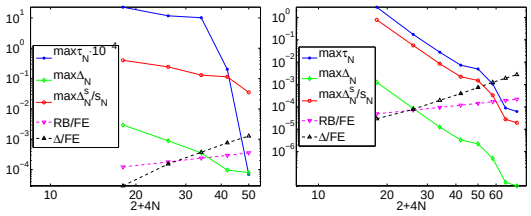

Figure 6. Online timings and maximum values of the error bound components (left: Gr–Pr, right: Gr–A). RB/FE is the ratio between a RB and a FE solve and Δ/FE is the ratio between the time needed for the error bound computation and a FE solve. On the left, τ_N has been divided by 10^4 for visualization reasons; on the left, $\max \tau_N$ is smaller than 1 only for $N = 12$

The initial conditions are $\boldsymbol{u} = 0$ and $T = 0$. The aspect ratio A of the cavity is equal to 4 and the left side and the right side of the cavity have the temperature equal to one and zero, respectively. Note we lift the temperature by the function $T_L = 1 - x_1/A$.

We consider the solution of these Boussinesq equations for $t_f = 0.15$ and $\mathrm{Gr} \in [0.5\cdot 10^5, 2\cdot 10^5]$, $\mathrm{Pr} \in [0.01, 0.05]$. Our parameter is $\boldsymbol{\mu} \equiv (\boldsymbol{\mu}_1, \boldsymbol{\mu}_2) \equiv (\mathrm{Gr}, \mathrm{Pr})$, which implies that the parameter domain $\mathcal{D}$ is equal to $[0.5\cdot 10^5, 2\cdot 10^5] \times [0.01, 0.05]$. The final time t_f and the parameter domain $\mathcal{D}$ are sufficiently large to observe (almost) steady states, the onset of oscillatory instability, and supercritical unsteady regimes. Note that we choose the particular "balanced" scaling of variables and equations — one of many possible classical options for distributing the parameters — in order to obtain better *a posteriori* error estimates for the subsequent reduced basis approximation.

Our particular interest is not in the solution field *per se*, but rather in the output s representing a local average-velocity. This output can be expressed as a functional of the x_1-velocity, namely, $s(t;\boldsymbol{\mu}) = \frac{1}{\sqrt{\boldsymbol{\mu}_1\boldsymbol{\mu}_2}|D|}\int_D u_1(t;\boldsymbol{\mu})$; here $D = [1.81, 2.20] \times [0.60, 0.67]$, the shaded area in Figure 3, is the subdomain over which the x_1 velocity is averaged. Note that the output $s(t;\boldsymbol{\mu})$, as scaled, can be interpreted as an effective Reynolds number — a measure of nonlinearity.

We can interpret our model problem as a "response to disturbance." We commence initially with no flow and uniform temperature conditions $\tilde{T}_{\mathrm{hot}} = \tilde{T}_{\mathrm{cold}}$ everywhere. We then abruptly increase $\tilde{T}_{\mathrm{hot}}$ which, given $\mathrm{Pr} \ll 1$, rapidly produces the conduction equilibrium temperature distribution T_L — for simplicity we assume this field is established instantaneously and hence impose (*perturbation* temperature) $T(x,0) = 0$. The flow then responds via buoyancy to (and of course subsequently affects) the temperature distribution. We measure the parametric dependence of this response through our output $s(\boldsymbol{\mu}, t)$.

The Finite Element "truth" approximation is modeled by a classical $\mathbb{P}_2 - \mathbb{P}_1 - \mathbb{P}_2$ (quadratic/linear/quadratic) Taylor-Hood spatial discretization with a total of $\mathcal{N} = 6{,}371$ veloc-

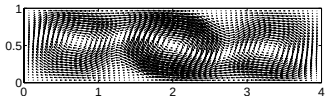

Figure 7. The streamline of the velocity at $t^k = 0.10$ for $(\mathrm{Gr},\mathrm{Pr}) = (2.0\times10^5, 0.02)$.

ity, pressure, and temperature degrees-of-freedom and a Crank-Nicholson temporal discretization with constant time step $\Delta t = .0005$ (corresponding to $K = 300$ time levels for our final time $t_f = 0.15$). We show in Figure 7 the streamline of the velocity field corresponding to $(\mathrm{Gr},\mathrm{Pr}) = (2\times10^5, 0.02)$. Clearly, the flow field exhibits very interesting dynamics with multiple cell patterns.

We present in Figure 8 the scaled vertical velocity at the spatial point $x = (2, 0.8)$ as a function of time t^k for both the "truth" and the RB approximation for $(\mathrm{Gr},\mathrm{Pr}) = (2\times10^5, 0.01)$. Despite the complex behavior of the flow and the relatively wide range of $(\mathrm{Gr},\mathrm{Pr})$, the RB approximation accurately captures the dynamics of the truth finite element solution — re-equilibration below $\mathrm{Gr}_{\mathrm{cr}}$ and oscillatory growth above $\mathrm{Gr}_{\mathrm{cr}}$ — with only relatively few ($N = 60$) basis functions. We can attribute this rapid convergence to the Galerkin projection and the effectiveness of the POD-Greedy sampling procedure; the latter can be viewed as a systematic parametric extension of earlier POD model reduction approaches [5] to flow problems.

Finally, we turn to a more realistic "real-time" context. We show in Figure 9 the RB output $s_N(t^k;\boldsymbol{\mu})$ and output bounds $s_N^{\pm}(t^k;\boldsymbol{\mu}) = s_N(t^k;\boldsymbol{\mu}) \pm \Delta_N^s(t^k;\boldsymbol{\mu})$ as a function of t^k for $(\mathrm{Gr},\mathrm{Pr}) = (2\times10^5, 0.01)$ for $N = 40$ and $N = 80$. We observe good convergence and meaningful/useful rigorous error bounds. Furthermore we note that, even for $N = 80$, Online calculation of the RB output $s_N(t^k;\boldsymbol{\mu})$ (respectively, the RB output error bound $\Delta_N^s(t^k;\boldsymbol{\mu})$), $1 \le k \le K$, is roughly 1,100× faster (respectively, 170× faster) than direct evaluation of the FE output $s^{\mathcal{N}}(t^k;\boldsymbol{\mu}), 1 \le k \le K$; and, for $N = 40$, Online calculation of $s_N(t^k;\boldsymbol{\mu})$ (respectively, $\Delta_N(t^k;\boldsymbol{\mu})$), $1 \le k \le K$, is roughly 2,400× faster (respectively, 750× faster) than direct evaluation of $s^{\mathcal{N}}(t^k;\boldsymbol{\mu})$, $1 \le k \le K$. We note that the Online time to evaluate the error bound $\Delta_N(t^k;\boldsymbol{\mu})$ is dominant because it has higher computational complexity than the RB output $s_N(t^k;\boldsymbol{\mu})$. We note that for natural convection problems in three space dimensions the RB savings will be even more significant.

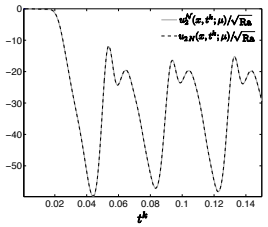

Figure 8. Comparison between the truth and RB ($N = 60$) scaled vertical velocity at the spatial point $x = (2, 0.8)$ as a function of time t^k for $(\mathrm{Gr},\mathrm{Pr}) = (2\times10^5, 0.01)$.

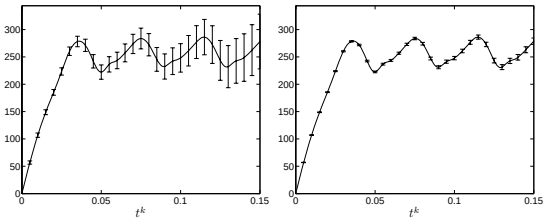

Figure 9. The reduced basis output $s_N(t^k;\boldsymbol{\mu})$ and output bounds $s_N^{\pm}(t^k;\boldsymbol{\mu}) = s_N(t^k;\boldsymbol{\mu}) \pm \Delta_N^s(t^k;\boldsymbol{\mu})$ as a function of t^k for $(\mathrm{Gr},\mathrm{Pr}) = (2.0\times10^5, 0.01)$ for $N = 40$ (left), and $N = 80$ (right).

REFERENCES

[1] B. O. Almroth, P. Stern, and F. A. Brogan, 1978. "Automatic choice of global shape functions in structural analysis" *AIAA Journal* **16** pp. 525–528.

[2] V.S. Arpaci, 1966. *Conduction heat transfer*. Addison-Wesley , Reading, UK.

[3] V. S. Arpaci, P. S. Larsen, 1984, *Convection heat transfer*. Prentice Hall, Englewood Cliffs, US.

[4] F. Brezzi, J. Rappaz, and P.A. Raviart, 1980. "Finite dimensional approximation of nonlinear problems. Part I: Branches of nonsingular solutions". *Numerische Mathematik*, **36**, pp. 1–25.

[5] A.E. Deane, I.G. Kevrekidis, G.E. Karniadakis, and S.A. Orszag, 1991. "Low-dimensional models for complex geometry flows: Application to grooved channels and circular cylinders", *Phys. Fluids*, **10**, pp. 2337–2354.

[6] S. Deparis, 2008. "Reduced basis error bound computation of parameter-dependent Navier–Stokes equations by the natural norm approach", *SIAM Journal of Numerical Analysis*, **46** (4), pp. 2039–2067.

[7] S. Deparis, G. Rozza, 2009. "Reduced basis method for multi-parameter dependent steady Navier–Stokes equations: applications to natural convection in a cavity", to appear on *J. Comp. Phys*.

[8] A. Yu. Gelfgat, P. Z. Bar-Yoseph, and A. L. Yarin, 1999. "Stability of multiple steady states of convection in laterally heated cavities", *Journal of Fluid Mechanics*, **388**, pp. 315–334.

[9] M. A. Grepl, Y. Maday, N. C. Nguyen, A. T. Patera, 2007. "Efficient reduced-basis treatment of nonaffine and nonlinear partial differential equations". *M2AN (Math. Model. Numer. Anal.)* **41** (3), pp. 575–605.

[10] M. A. Grepl, A. T. Patera, 2005. "*A Posteriori* error

bounds for reduced-basis approximations of parametrized parabolic partial differential equations". *M2AN (Math. Model. Numer. Anal.)* **39** (1), pp. 157–181.

[11] M. D. Gunzburger, J. Peterson and J. N. Shadid, 2007, "Reduced-order modeling of time-dependent PDEs with multiple parameters in the boundary data", *Comp. Meth. Applied Mech*, **196** (4)-(6), pp.1030–1047.

[12] B. Haasdonk and M. Ohlberger, 2008. "Reduced Basis Method for Finite Volume Approximations of Parametrized Evolution Equations", *Mathematical Modelling and Numerical Analysis (M2AN)*, **42** (2), pp. 277–302.

[13] D. B. P. Huynh, G. Rozza, S. Sen, A. T. Patera, 2007. "A successive constraint linear optimization method for lower bounds of parametric coercivity and inf-sup stability constants". *C. R. Acad. Sci. Paris, Analyse Numérique* **345** (8), pp. 473–478.

[14] D. B. P. Huynh, C. N. Nguyen, G. Rozza, A. T. Patera, 2007-09, Documentation for rbMIT Software.`http://augustine.mit.edu/methodology/methodology_rbMIT_System.htm` ©MIT, Tech. Lic. Office 12600, Cambridge, MA, US.

[15] K. Ito and S. S. Ravindran, 2001. "Reduced Basis Method for Optimal Control of Unsteady Viscous Flows", *International Journal of Computational Fluid Dynamics*, **15** (2), pp.97–113.

[16] P. S. Johansson, H.I. Andersson and E.M. Rønquist, 2006, "Reduced-basis modeling of turbulent plane channel flow", *Computers and Fluids*, **35** (2), pp.189–207.

[17] N. C. Nguyen, A. T. Patera, 2009. "Reduced basis approximation and A Posteriori error estimation for the parametrized unsteady Boussinesq equations: application to natural convection in a laterally heated cavity". *Journal of Computational Physics*, submitted.

[18] N. C. Nguyen, G. Rozza, D. B. P. Huynh, A. T. Patera, 2009. "Reduced basis approximation and a posteriori error estimation for parametrized parabolic pdes; Application to real-time Bayesian parameter estimation". In *Computational Methods for Large Scale Inverse Problems and Uncertainty Quantification*. L. Biegler *et al.* (eds.), John Wiley and Sons, UK.

[19] N. C. Nguyen, G. Rozza, A. T. Patera, 2009. "Reduced basis approximation and a posteriori error estimation for the time-dependent viscous Burgers equation", Submitted to Calcolo.

[20] N. C. Nguyen, K. Veroy and A. T. Patera, 2005. "Certified real-time solution of parametrized partial differential equations". In *Handbook of Materials Modeling*, S. Yip (ed.), Springer, New York, pp. 1523–1558.

[21] A. K. Noor, J. M. Peters, 1980. "Reduced basis technique for nonlinear analysis of structures", *AIAA Journal*, **18** (4), pp. 455–462.

[22] A. K. Noor, C. D. Balch and M. A. Shibut, 1984. "Reduction methods for non-linear steady-state thermal analysis", *Int. J. Num. Meth. Engrg.*, **20**, pp. 1323–1348.

[23] T. A. Porsching, 1985. "Estimation of the error in the reduced basis method solution of nonlinear equations", *Mathematics of Computation*, **45** (172), pp. 487–496.

[24] J. S. Peterson, 1989. "The reduced basis method for incompressible viscous flow calculations", *SIAM J. Sci. Stat. Comput.*,**10** (4), pp. 777–786.

[25] C. Prud'homme, D. Rovas, K. Veroy, Y. Maday, A. T. Patera and G. Turinici, 2002, "Reliable real-time solution of parametrized partial differential equations: reduced-basis output bound methods", *Journal of Fluids Engineering*, **124** (1), pp. 70–80.

[26] A. Quarteroni and G. Rozza, 2007. "Numerical Solution of parametrized Navier-Stokes equations by reduced basis method", *Num. Meth. PDEs*, **23** (4), pp. 923–948.

[27] A. Quarteroni, A. Valli, 1997. *Numerical Approximation of Partial Differential Equations*, 2nd ed., Springer-Verlag, Berlin.

[28] B. Roux (ed.) 1990. *Numerical simulation of oscillatory convection in low-Pr fluids: A GAMM Workshop*, Notes on Numerical Fluid Mechanics, vol. 27. Vieweg, Braunschweig.

[29] G. Rozza, D. B. P. Huynh, N. C. Nguyen, A. T. Patera, 2009. "Real-time reliable simulation of heat transfer phenomena", *Proceedings of ASME HT2009*, paper HT2009-88212, Submitted.

[30] G. Rozza, D. B. P. Huynh, A. T. Patera, 2008. "Reduced basis approximation and a posteriori error estimation for affinely parametrized elliptic coercive partial differential equations: Application to transport and continuum mechanics", *Archives Computational Methods in Engineering*, **15** (3), pp. 229–275.

[31] G. Rozza, K. Veroy, 2007. "On the stability of the reduced basis method for Stokes equations in parametrized domains", *Comput. Methods Appl. Mech. Engrg.*, **196** (7), pp. 1244–1260.

[32] W. E. Schiesser, C. A. Silebi, 1997, *Computational Transport Phenomena: Numerical Methods for the Solution of Transport Problems*. Cambridge Univeristy Press, Cambridge, UK.

[33] S. Sen, K. Veroy, D. B. P. Huynh, S. Deparis, N. C. Nguyen and A. T. Patera, 2006. "Natural norm" a posteriori error estimators for reduced basis approximations", *Journal of Computational Physics*, **217** (1), pp. 37–62.

[34] K. Veroy, A. T. Patera, 2005. "Certified real-time solution of the parametrized steady incompressible Navier-Stokes equations; Rigorous reduced-basis *a posteriori* error bounds", *International Journal for Numerical Methods in Fluids*, **47**, pp. 773–788.